



COVID-19 Research Tools

Defeat the SARS-CoV-2 Variants

InvivoGen



This information is current as of February 24, 2022.

FcγRIIb on Liver Sinusoidal Endothelium Clears Small Immune Complexes

Latha P. Ganesan, Jonghan Kim, Yun Wu, Sudhasri Mohanty, Gary S. Phillips, Daniel J. Birmingham, John M. Robinson and Clark L. Anderson

J Immunol 2012; 189:4981-4988; Prepublished online 10 October 2012;

doi: 10.4049/jimmunol.1202017

<http://www.jimmunol.org/content/189/10/4981>

References This article **cites 47 articles**, 14 of which you can access for free at:
<http://www.jimmunol.org/content/189/10/4981.full#ref-list-1>

Why *The JI*? Submit online.

- **Rapid Reviews! 30 days*** from submission to initial decision
- **No Triage!** Every submission reviewed by practicing scientists
- **Fast Publication!** 4 weeks from acceptance to publication

**average*

Subscription Information about subscribing to *The Journal of Immunology* is online at:
<http://jimmunol.org/subscription>

Permissions Submit copyright permission requests at:
<http://www.aai.org/About/Publications/JI/copyright.html>

Email Alerts Receive free email-alerts when new articles cite this article. Sign up at:
<http://jimmunol.org/alerts>



FcγRIIb on Liver Sinusoidal Endothelium Clears Small Immune Complexes

Latha P. Ganesan,* Jonghan Kim,[†] Yun Wu,[‡] Sudhasri Mohanty,* Gary S. Phillips,[§] Daniel J. Birmingham,* John M. Robinson,[¶] and Clark L. Anderson*

It has long been known that the ITIM-bearing IgG Fc receptor (FcγRIIb, RIIb) is expressed on liver sinusoidal endothelial cells (LSEC) and that the liver is the major site of small immune complex (SIC) clearance. Thus, we proposed that RIIb of LSEC eliminates blood-borne SIC, thereby controlling immune complex-mediated autoimmune disease. Testing this hypothesis, we found most RIIb of the mouse, fully three-quarters, to be expressed in liver. Moreover, most (90%) liver RIIb was expressed in LSEC, the remainder in Kupffer cells. An absent FcγR in LSEC implied that RIIb is the sole FcγR expressed. Testing the capacity of liver RIIb to clear blood-borne SIC, we infused mice intravenously with radio-iodinated SIC made of OVA and rabbit IgG anti-OVA. Tracking decay of SIC from the blood, we found the RIIb knockout strain to be severely deficient in eliminating SIC compared with the wild-type strain, terminal half-lives being 6 and 1.5 h, respectively. RIIb on LSEC, a major scavenger, keeps SIC blood concentrations low and minimizes pathologic deposition of inflammatory immune complex. *The Journal of Immunology*, 2012, 189: 4981–4988.

It is an axiomatic function of the immune system that complexes of Ag and Abs are eliminated efficiently from the bloodstream, ridding the body of harmful elements of a variety of sorts, both invasive and endogenous. A number of features of immune complexes govern their elimination, the most obvious being size. Large immune complexes composed of, for example, bacteria-size microorganisms and blood cells coated with Ab are removed by cells of the mononuclear phagocyte system by the process of receptor-mediated phagocytosis. These complexes are sometimes referred to as “insoluble” because they readily sediment at low gravity forces.

Likewise, small immune complexes (SIC), the size of serum proteins complexed with corresponding Ab, are in most situations eliminated efficiently from the blood, specifically by the cells of the classical reticuloendothelial system, chiefly by the sinusoidal cells of the liver (1–4). These SIC are often termed “soluble” because they fail to sediment at low gravity forces; experimentally, they are prepared at “antigen excess,” at concentrations of Ag exceeding that required for the optimal preparation of insoluble

immune complexes (5). In certain circumstances, however, these SIC fail to be eliminated and go on to produce disease. The pathophysiology of such immune complex-mediated diseases has been the focus of considerable experimental interest over the past century. Intensive study of the mechanisms of these diseases, beginning with experimental models of serum sickness in the 1950s most prominently by Dixon and colleagues (6), Benacerraf and colleagues (7), and others, has led to the current concept that SIC must accrete to a certain requisite size to deposit in critical organs, such as the kidney, where they produce inflammation and disease (8–11). Thus, analyzing the mechanism by which immune complexes, while still small, are eliminated by the liver becomes an imperative theoretical and practical objective.

A crucial clue to the mechanism of SIC elimination emerged 30 y ago when it was observed that mab 2.4G2, specific for the binding sites of all mouse FcγR, blocked liver uptake of SIC infused intravenously into mice (3). This finding implicated liver sinusoidal FcγR in the elimination of SIC. Many concluded that the Kupffer cells (KC) were responsible for such liver elimination. Rather, as we have recently found, liver sinusoidal endothelial cells (LSEC) expressing FcγRIIb (RIIb) are responsible for virtually all mab 2.4G2 binding in mouse liver (12). Several converging lines of recent evidence (4, 12–18) now indicate that the predominant FcγR on LSEC is RIIb, the low-affinity ITIM-bearing inhibitory receptor studied most carefully on B cells, macrophages, and dendritic cells (reviewed in Refs. 19, 20).

We are led by the evidence presented above to propose that RIIb expressed on LSEC are responsible for the ongoing removal of SIC from the blood. This hypothesis has two predictions; first, that liver expression of RIIb is remarkably abundant; second, that a mouse strain lacking RIIb will fail to remove SIC from blood. We tested these two predictions, the first by immunofluorescence microscopy and immunoblotting, measuring the expression of RIIb in liver compared with the entire animal; and the second by comparing the rates of elimination of radio-iodinated SIC from the blood in wild-type (WT) and RIIb knockout (KO) strains of mice.

Neither test rejected the hypothesis. Rather, a very high fraction, fully three-quarters, of total body RIIb was found in the liver, most

*Department of Internal Medicine, The Ohio State University, Columbus, OH 43210; [†]Harvard School of Public Health, Boston, MA 02115; [‡]National Science Foundation Nanoscale Science and Engineering Center for Nanoengineering of Polymer Biomedical Devices, The Ohio State University, Columbus, OH 43210; [§]Department of Biostatistics, The Ohio State University, Columbus, OH 43210; and [¶]Department of Physiology and Cell Biology, The Ohio State University, Columbus, OH 43210

Received for publication July 20, 2012. Accepted for publication September 13, 2012.

This work was supported in part by National Institutes of Health Grant R01 HD38764.

Address correspondence and reprint requests to Dr. Clark L. Anderson, Department of Internal Medicine, The Ohio State University, 012K Davis Heart and Lung Research Institute, 473 West Twelfth Avenue, Columbus, OH 43210. E-mail address: anderson.48@osu.edu

Abbreviations used in this article: BMM, bone marrow macrophage; DIC, differential interference contrast; DLS, dynamic light scattering; IF, immunofluorescence; KC, Kupffer cell; KO, knockout; LSEC, liver sinusoidal endothelial cell; MR, mannose receptor; POE, point of equivalence; RIIb, FcγRIIb (Fcγ receptor of the IIb subclass); SIC, small immune complex; WT, wild-type.

Copyright © 2012 by The American Association of Immunologists, Inc. 0022-1767/12/\$16.00

on LSEC. Further, the removal rate of SIC from blood of RIIb KO mice compared with WT mice was severely curtailed. These results confirm our hypothesis and suggest new ways of conceptualizing and treating immune complex-mediated diseases.

Materials and Methods

Ethics statement and animals

Male mice of age 12–15 wk were obtained from Taconic Laboratory. They were of strains BALB/c WT and RIIb KO on a BALB/c background [C.129S4 (B6)-*Fcgr2b*^{tm1TrK}/cAnNTac N12C.129S4 and model number 580-MJ]. The RIIb KO mice were generated and described previously (21). All protocols were approved by The Ohio State University Institutional Animal Care and Use Committee. Bleedings were performed under isoflurane anesthesia, and all efforts were made to minimize suffering.

Cells

RAW 264.7, A20, and COS-7 cells were obtained from American Type Culture Collection. COS-7 cells were maintained in DMEM supplemented with 10% FBS. RAW 264.7 and A20 cells were maintained in RPMI 1640 medium supplemented with 5% FBS. Bone marrow macrophages (BMM) were obtained and differentiated with M-CSF as previously described (22).

Quantitative immunoblot

The expression of RIIb and Syk in various organs was quantified by immunoblot as follows: organs (kidney, spleen, ileum, liver, heart, and lung) from three sacrificed mice were removed and weighed. Small pieces of ~100 µg from each organ were homogenized with a glass homogenizer in a lysis buffer composed of 25 mM HEPES, 20 mM Na₄H₂O₇·10H₂O, 100 mM NaF, 4 mM EDTA, 2 mM Na₃VO₄, 1% Triton X-100, 0.34 mg/ml PMSF, 0.01 mg/ml aprotinin, and 0.01 mg/ml leupeptin. Lymph nodes from axillary, mesangial, inguinal, and submandibular regions were pooled. Bone marrow cells were flushed from femurs, centrifuged at 376 × *g* for 5 min, and lysed. Blood (~80 µl) was obtained from three mice via the retro-orbital plexus using heparinized capillary pipettes, and the erythrocytes were lysed by dilution in 10 vol of 20% PBS at room temperature for 10 min. Cells remaining were spun down at 376 × *g* for 5 min and lysed. All lysates were incubated on ice for 30 min and centrifuged at 18,407 × *g* for 15 min. The protein concentrations of spun lysates were estimated using the bicinchoninic acid protein assay.

Organ lysates (35 µg) along with lysates of control standards (0, 3, 6, 9, and 12 µg of lysates from A20 cell line for RIIb blots and 0, 5, 10, 15, 20 µg of lysates from RAW 264.7 cells for Syk blots) were separated on 8–16% gradient SDS-polyacrylamide gels, and the proteins were transferred to nitrocellulose membranes (0.45 µm). The membranes were blocked with 5% milk for 30 min and then incubated overnight with primary rabbit anti-mouse RIIb (kind gift from John Cambier) and rabbit anti-Syk (Santa Cruz Biotechnology) Abs at concentrations of 1:5000 at 4°C. The bands were developed using Alexa Fluor 488-conjugated goat anti-rabbit IgG Ab at a concentration of 1:1000 and detected for quantification using a laser scanner (Pharos-FX; Bio-Rad).

Band intensities were quantified using Quantity One software from Bio-Rad. The RAW and A20 cell-equivalent concentrations of RIIb and Syk, respectively, were calculated from standard curves after subtracting background. The total amounts of RIIb and Syk in all organs were calculated by factoring the weights of the respective organs and the respective volumes of lysis buffer and were plotted as percentages of total after normalizing to the organ with the lowest signal within each experiment. For statistical analysis, protein expression was natural log-transformed to normalize the distribution and to stabilize the variance across organ type (homoscedasticity assumption). Using a mixed-effects linear regression model where the subject is the random effect and the organ type is the fixed effect, we compared the RIIb protein expression in the liver to the average of the other eight organs. Similarly, we compared the Syk protein expression in the spleen to the average of the other eight organs.

Equal protein loading of all organ lanes was ensured by the following strategies: First, equal amounts of protein lysates (bicinchoninic acid assay) were loaded into each gel well. Second, densitometry of the Coomassie blue-stained gel showed that total densities of all bands in an organ lane except blood were no more than 2-fold different from the mean organ density, and blood was 3.4 times less than the mean. Third, reblotting the immunoblot from Fig. 1 with goat anti-actin Ab (Santa Cruz Biotechnology) and analyzing the actin bands by densitometry using ImageJ software showed that save for the blood sample where actin was present but low, the density of the actin bands from any of the organs was less than 2-fold

different from the mean density of all actin bands. The literature records similar variation to ours when comparing organs (23–25). Erythrocyte ghost proteins are known to stain poorly with Coomassie (26).

For visual representation alone (Fig. 1A), as opposed to quantification (Fig. 1B), 50 µg of tissue lysates were separated on 10% linear SDS-polyacrylamide gels, transferred, probed with Ab. developed by ECL, and imaged. The lysates from cell lines A20, RAW 264.7, and BMM differentiated using M-CSF were used as control sources of b1 and b2 protein isoforms.

Immunofluorescence

Small pieces of liver (~5 mm) were fixed in 4% paraformaldehyde in PBS for 2 h at room temperature and, after washing with PBS, were infused in 20% sucrose–PBS overnight at 4°C. The tissues were then embedded in a freezing medium and stored at –80°C. Cryostat sections, 5 µm thickness, were blocked in 5% milk–PBS prior to incubation overnight at 4°C with primary Abs. The primary Abs rabbit anti-mouse RIIb, goat anti-mouse RIIb (kind gift from Mark Coggeshall), rabbit anti-mannose receptor (Santa Cruz Biotechnology), and rabbit anti-Fcγ-chain (Millipore) were all used at dilutions of 1:25. The mab 2.4G2 was used at a concentration of 20 µg/ml. After three washes with PBS, the sections were incubated with secondary Abs for 1 hr at room temperature. Nuclei were stained with DAPI for 10 min, and the sections were mounted under coverslips in Prolong gold (Invitrogen). Control incubations included isotype controls along with their respective secondary Abs and also secondary Abs alone. The images were acquired in the Olympus FluoView 1000 Laser Scanning Confocal Microscope equipped with a spectral detection system for a finer separation of fluorochromes (FV 1000 spectra) using a ×60 oil immersion lens at room temperature. Image analyses were done using FluoView software (Olympus version 2.1.39). In Fig. 4, to overcome the inherent limits of resolution in the z-dimension in our confocal microscopes, we used ultrathin cryosections of liver tissue as the substratum for high-resolution immunofluorescence microscopy as we have described (27–29). Preparation of tissue and ultrathin cryosections we described in detail earlier (30).

Quantitative microscopy

The relative liver expression of RIIb between LSEC and KC, shown in Fig. 3 (bottom row), was quantified from immunofluorescence images dual-stained for RIIb (green) using goat anti-RIIb Ab and anti-F4/80 (red) in the following manner. The total intensity of RIIb (green) in the images was calculated using ImageJ software. From this total was subtracted the intensity of RIIb measured in all cropped KC, identified with F4/80. Thus, total intensity of RIIb minus KC intensity of RIIb equaled the RIIb intensity of LSEC. Optical sections with a total area of 6.3 mm² were analyzed from each of three different mice.

The fluorescence intensities from mannose receptor (MR) (green) and RIIb (red) channels in the ultrathin sections represented in Fig. 4 were obtained using LSM 510 META software. Randomly selected sinusoids (*n* = 100) from merged color images were cross-sectioned eight times at 45° angles, and the intensities of both color channels of eight sections over the LSEC cross-sectional distance from luminal to abluminal surface were recorded. Data were analyzed using a paired *t* test.

Immunofluorescence from anti-Fcγ-chain (green) was colocalized with signals from mab F4/80 and mab 2.4G2 (Fig. 6) in 60 immunofluorescence optical sections with an area of 12.6 mm² from a total of three mice. Using Olympus FV10-ASW analysis software, the Mander's overlap coefficient *R* was obtained and expressed as a percentage of colocalization (31).

Immunofluorescence signal from mab 2.4G2 colocalized with signal from rabbit anti-RIIb shown in the top row of Fig. 2 was quantified as described for Fig. 6, with the following modification. Individual LSEC (*n* = 60) were cropped from images obtained from two WT livers, and Mander's overlap coefficient was expressed as percent colocalization. By cropping the LSEC, we avoided pixels from nuclei nonspecifically stained with the rabbit RIIb Ab. Signal from mab 2.4G2 colocalization with immune fluorescence from goat anti-RIIb in individual LSEC (*n* = 194) was quantified manually by scoring the number of LSEC that were positive for 2.4G2 (green) and goat anti-RIIb (red) (Fig. 2, bottom row).

RT-PCR

Total RNA extracted from TRIzol lysates of organs and cell lines were transcribed to cDNA using Thermoscript RNase H-reverse transcriptase and amplified using primers specific for mouse RIIb. The RNA isolation protocol, primer sequences, and PCR conditions were described earlier (32). The RT-PCR products were resolved by electrophoresis on 1.5% agarose gels, stained with ethidium bromide, and imaged using Quantity One software.

Quantitative precipitin reaction and small immune complex preparation

A single lot of affinity-purified rabbit IgG anti-OVA Ab (Immunology Consultants) was "calibrated" for its interaction with OVA (Sigma) by a quantitative precipitin reaction to derive a point of equivalence (POE) (2, 5, 33). Specifically, microfuge tubes containing serially diluted OVA at concentrations ranging from 6.5 to 156 $\mu\text{g}/\text{ml}$ were each incubated with 200 $\mu\text{g}/\text{ml}$ rabbit anti-OVA Ab in a total volume of 500 μl of PBS at pH 7.4 for 1 h at room temperature and 18 h at 4°C. The mixtures were centrifuged at $2000 \times g$ for 10 min; the pellets were dissolved in glycine HCl buffer (0.05 M glycine and 0.15 M NaCl pH 2.3); and the protein concentrations of pellets and supernatants were determined by UV absorbance at 280 nm.

The calibration curve of the precipitin reaction yielded a distinct POE at Ag and Ab concentrations of 26 and 200 $\mu\text{g}/\text{ml}$, respectively. To prepare SIC for determination of particle size by dynamic light scattering (DLS) and for infusion into mice, we increased the protein concentrations 5-fold greater than the concentration used in the precipitin curve. SIC were prepared by mixing rabbit anti-OVA Ab at 1000 $\mu\text{g}/\text{ml}$ ($\sim 5 \times 200$) with OVA (Ag) at 1950 $\mu\text{g}/\text{ml}$ ($26 \times 5 \times 15$), a 15-fold excess over the POE Ag concentration determined in the calibration curve, attempting to duplicate the conditions used by others (2, 3, 7). The mixture was incubated for 1 h at room temperature and 18 h at 4°C and was centrifuged at $2000 \times g$ for 1 min. SIC size was measured by DLS. To prepare trace-labeled SIC for infusion into mice, radio-iodinated rabbit anti-OVA Ab (iodinated as described later) was added to unlabeled Ab at a 1:500 mass ratio prior to mixing Ag with Ab exactly as described earlier.

Radio-iodination of Ab

Affinity-purified rabbit IgG anti-OVA Ab was dialyzed against PBS pH 7.4 containing 1.06 mM KH_2PO_4 , 155 mM NaCl, and 2.97 mM $\text{Na}_2\text{HPO}_4 \cdot 7\text{H}_2\text{O}$ and radio-iodinated by a modified chloroglycouril method using chloroglycouril-coated tubes (Pierce). Briefly, at room temperature 1 μCi of Na^{125}I (Pierce) was activated in a chloroglycouril-coated tube for 6 min, and the activated Na^{125}I was transferred to 100 μl of Ab at 1.5 mg/ml. The iodination reaction was terminated at 9 min by adding 50 μl of 10 mg tyrosine/ml in PBS at pH 7.4. The radio-iodinated Ab was separated from free radio-iodine using PD-10 desalting columns equilibrated with 0.1% fish gelatin in PBS. The precipitability of labeled Ab in 12.5% iced TCA was $>95\%$. Labeling efficiency was $\sim 50\%$. The cpm/ μg of Na^{125}I -labeled Ab was 1.4×10^7 and 3.2×10^6 in two experiments.

Analysis of SIC using DLS

The particle size of SIC was estimated by DLS (BI-200SM Research Goniometer System; Brookhaven Instrument, Holtsville, NY) under the following conditions: detection angle 90° , laser wavelength 633 nm, temperature 20°C , measurement duration 2 min. The particles were diluted in 0.22- μm -filtered PBS. Fe_3O_4 particles of size range 200–250 (BD Biosciences), 10, and 5 nm (NN Laboratories) were analyzed to check the precision of the instrument and were found to have mean diameters of 209, 12, and 20 nm, respectively, suggesting imprecision at low particle size. The standard latex particles of size 40, 92, and 100 nm were found to have mean diameters of 42, 93, and 98 nm, respectively. The mean diameters by volume of Ag and Ab at a concentration of 1 mg/ml were 6 ± 1 and 5 ± 1 nm, mean \pm variance of two observations, respectively. The mean diameter by volume of particles at the POE was 1228 ± 774 nm. The mean diameter by volume of SIC particles prepared at 3-fold excess Ag was measured to be 220 ± 14 nm. The characterization of SIC prepared at 15-fold excess Ag is presented in Fig. 7B and the text. All samples showed a monodispersed distribution with insignificant outliers and aggregates.

Clearance kinetics of SIC

To characterize *in vivo* SIC clearance kinetics, we infused by tail vein freshly prepared radio-iodinated SIC containing 1.4×10^6 and 1.9×10^6 cpm in 58 μl . Two identical experiments were performed 3 mo apart, in each infusing three WT and three RIIb KO mice matched for sex and age. The mice were bled of ~ 15 μl blood via the retro-orbital plexus at post-infusion times of 1, 5, 10, 20, 30, and 60 min. To adjust for different body weights of individual mice, the blood concentrations of radioactive SIC (cpm/10 μl blood) were normalized to an average value of dose/body weight among animals (i.e., a dose of 1.6×10^6 cpm/25.43 g body weight). Because a semilog plot of blood concentrations of iodinated SIC from both strains indicated biphasic decay, we used a biexponential decay model to fit the SIC concentration–time profile. Half-lives were calculated

by $0.693/(-\text{slope})$, where the slope was obtained from the biexponential decay analysis. Independent two-sample *t* test was performed to compare the means of two genotypes. Differences between WT and KO strains were considered significant at $p < 0.05$.

Quantification of SIC in various organs

Mice ($n = 3$) were infused intravenously with freshly prepared radio-iodinated SIC containing 1.1×10^6 cpm in 58 μl and were sacrificed at 25 min. The mice were bled of ~ 20 μl via the retro-orbital plexus; organs (liver, kidney, lung, spleen, and heart) were removed and weighed. SIC in the weighed portions of each organ were measured and quantified after factoring total organ weight.

Results

Most RIIb of the mouse is in the liver

We recently noticed that the expression of RIIb on LSEC was astonishingly high, far in excess of what we had perceived to be expressed on other RIIb reservoirs of the body such as spleen, lymph nodes, B cells, and macrophages (12). More precisely, assessing in our mind's eye the brightness and extent of RIIb fluorescence in a microscopic field of view of liver sections, and multiplying this by the three dimensions of the liver, the body's largest internal organ, the total quantity of RIIb would be far greater than that of any of the other RIIb sites of the body (data not shown). It has long been known that a like assessment of the human liver with a specific anti-RIIb Ab gives the identical impression by immunolabeling (14). Quantifying our visual impression, we measured by immunoblotting the expression of RIIb in lysates of the liver and spleen and most of the other major organs and tissues of the body (Fig. 1). Consistent with our visual impression, we found that of the total body pool of RIIb, fully $72 \pm 5\%$ ($n = 3$) was expressed in the liver, and the remaining 28% was spread among the other organs and tissues of the body, each being less than 10%. By mobility of the anti-RIIb identified bands, the liver appeared to express mostly the b2 protein isoform but also some b1, whereas, as expected, most of the RIIb in spleen was b1 (Fig. 1A). Our immunoblots of organ lysates affirm that this RIIb KO strain shows no evidence for the RIIb bands (data not shown). The band with b1 mobility in the kidney lane, as well as unidentified bands at 75 and 45 kDa in many lanes, were artifacts based on their presence in tissues from RIIb KO mice (data not shown). Further studies of kidney tissue sections examined by immunofluorescence (IF) microscopy with three anti-RIIb Abs showed no evidence for the expression of RIIb in the kidneys (data not shown).

Because our method of quantifying tissue expression of proteins from band densities in immunoblots entailed a large multiplication factor for liver due to its relative size, we also measured the expression of the tyrosine kinase Syk, reasoning that a molecule expressed largely in the spleen would appear highly expressed in liver if our method were artifactually amplifying the extent of liver expression (34). Confirming the validity of our method, $63 \pm 6\%$ of total body Syk was expressed in the spleen but less than 10% in liver and all other organs except the ileum (13%) where B cells and macrophages are prevalent (Fig. 1B).

LSEC expression of RIIb confirmed with three anti-RIIb Abs

Within the liver, RIIb is predominantly expressed in LSEC (12, 14, 17, 35). We confirmed this conclusion by IF microscopy using three anti-RIIb Abs; that is, mab 2.4G2 and two polyclonal Abs from goat and rabbit, the last directed toward the cytoplasmic tail sequence of RIIb. We found that all three Abs gave similar and mostly overlapping signals in LSEC (Fig. 2); these signals were specific for RIIb in that liver sections from RIIb KO mice showed

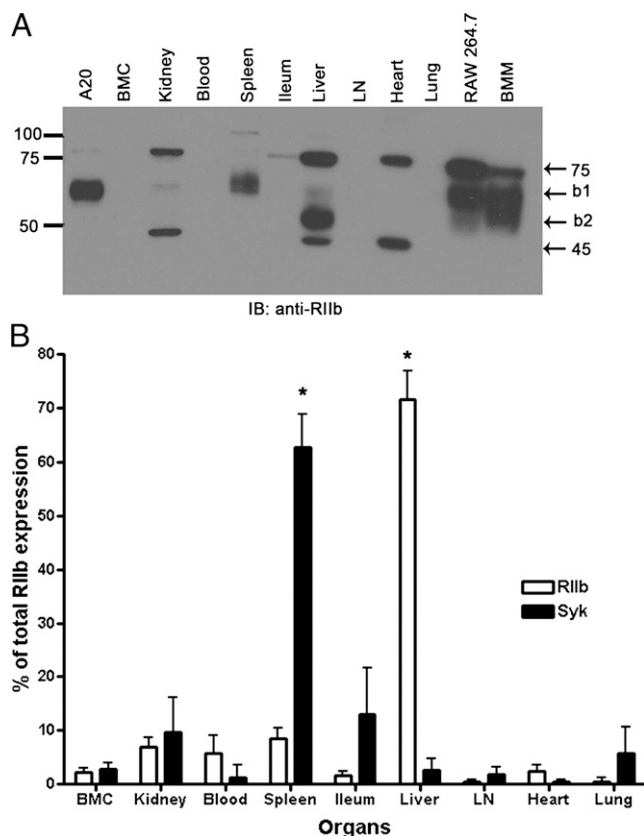


FIGURE 1. Most RIIb of mouse is in liver. **(A)** An ECL-developed immunoblot using rabbit anti-mouse RIIb Ab showing RIIb expression in several tissue and cell lysates prepared as described in *Materials and Methods*. Numbers are MW markers in kDa. **(B)** Bar graph expressing the means and SDs of immunoblot-derived band densities after factoring total organ weight for both RIIb isoforms and Syk from all organs ($n = 3$ WT mice). * $p < 0.001$ (expression levels of Syk and RIIb in spleen and liver, respectively, are statistically significantly different from the average of all other organs; see *Materials and Methods*). BMC, Bone marrow cells; LN, lymph nodes.

no LSEC binding (data not shown). None of these Abs gave positive signals with endothelium of portal and hepatic veins. All three Abs showed a weak staining pattern with KC as we reported earlier for mab 2.4G2 (12).

Within the liver, most RIIb is in LSEC

We quantified by IF microscopy of liver sections the relative expression of RIIb between LSEC and KC by colocalizing the binding of two anti-RIIb Abs with the KC marker F4/80 (Fig. 3). We found that of the total liver RIIb pixel intensity, 90% was expressed in LSEC and 10% in KC.

RIIb expression in LSEC predominates toward the apical membrane

Having earlier found that RIIb in the endothelium of the human placenta is expressed in the interior of the cell and not at the plasma membrane (28), we used the same strategy to localize RIIb in mouse LSEC, examining ultrathin (<100 nm) sections of liver by three-color IF microscopy, comparing anti-MR binding, which is relatively specific for LSEC (12), with anti-RIIb Ab binding (Fig. 4A). Quantifying the pixels of the two colors in merged images (Fig. 4B), we concluded that, unlike its localization in human placental endothelium, RIIb does not predominate in the interior of the cell; rather it appeared to be more highly expressed toward the apical portion of the LSEC, whereas MR was more diffusely spread throughout the cell.

The RIIb mRNA isoform expressed in liver is b2

Having found that LSEC-expressed RIIb constitutes nearly all RIIb of liver (Fig. 3), we realized that we could easily determine the mRNA isoform of RIIb in LSEC by RT-PCR analysis of whole-liver mRNA, comparing band sizes with known sizes from RIIb-expressing cells characterized earlier by others. Such an experiment indicated that the predominant isotype in liver was b2 with only a trace band of b1 being seen in the agarose gels (Fig. 5). We have analyzed the published cDNA sequence of rat RIIb from LSEC that was not isozymed in the original publication and find that the isotype was b2 and not b1 (17). Thus, human, rat, and mouse RIIb, which are highly expressed in LSEC, are of the b2 isotype (14, 16, 17).

Fcγ-chain is expressed only in KC and not in LSEC

We were unable to determine with confidence whether other members of the FcγR family were expressed in LSEC because of a dearth of reliable Abs to RI, RIII, and RIV that would be useful in IF microscopy. However, as all three of these agonist receptors require for function the association of the FcRγ-chain (36–38), we realized that by assessing FcRγ expression in LSEC, we could

FIGURE 2. LSEC expression of RIIb confirmed with three RIIb Abs. The confocal IF images in the *left column* show the binding pattern of anti-RIIb mab 2.4G2 (green). The *middle column* shows the staining pattern of two anti-RIIb Abs, rabbit polyclonal anti-mouse RIIb in the *top panel* and goat polyclonal anti-mouse RIIb in the *bottom panel* (both red). Note in the *top panel* that the nuclei were stained nonspecifically by the rabbit anti-RIIb Ab, as nuclei but not LSEC were stained in liver sections from RIIb KO strain (data not shown). The *right column* shows the merged color images of the *left- and middle-column* images plus differential interference contrast (DIC) and DAPI staining of nuclei. Scale bars, 10 μ m.

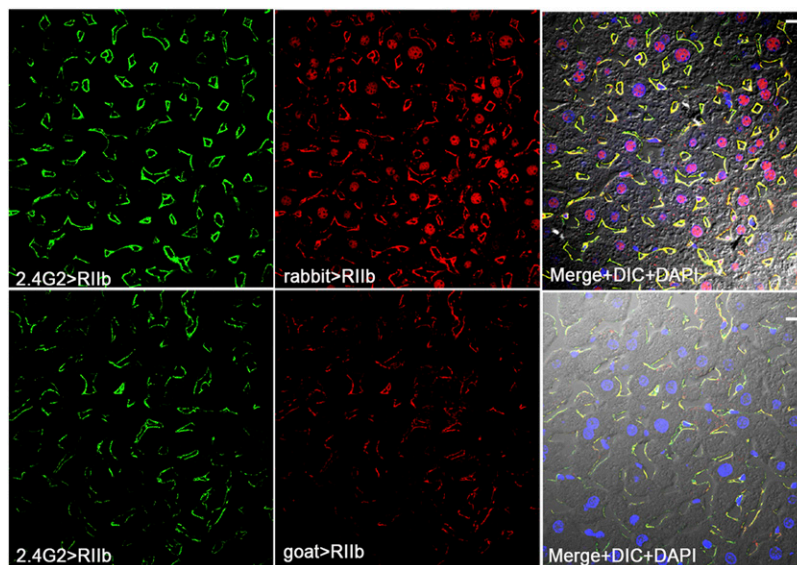
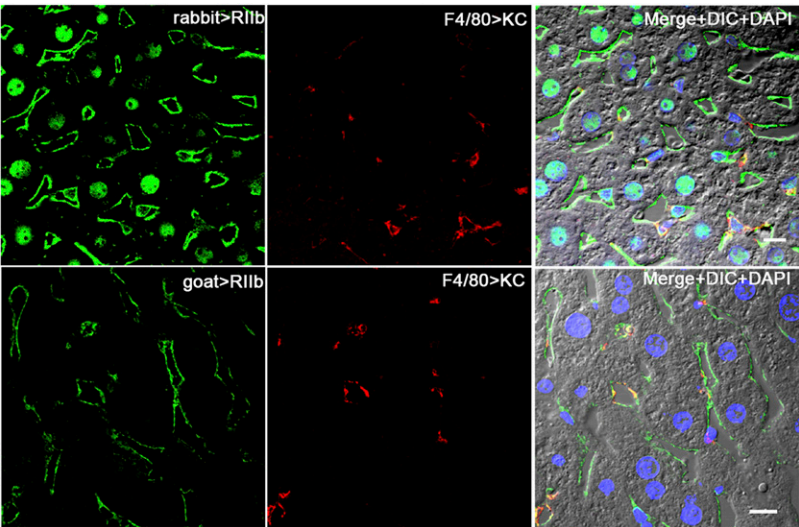


FIGURE 3. Within the liver, most RIIB is in LSEC. Confocal IF images in the *left column* show the binding pattern of rabbit anti-mouse RIIB in the *top panel* and goat anti-mouse RIIB in the *bottom panel* (both green). In the *middle column*, both panels show KC whereabouts with anti-F4/80 (red). The merged color images in the *right column* illustrate the relative abundance of RIIB expression in LSEC versus KC and show also DIC and DAPI staining of nuclei. Scale bars, 10 μ m.



indirectly assess the expression of the agonist members of the Fc γ R family in mouse. By three-color IF microscopy, we found FcR γ to be expressed only in the KC of the liver and not in the

LSEC (Fig. 6A). Quantifying the colored signals in these images, we affirmed that FcR γ was a distinctive feature of KC and not LSEC (Fig. 6B). Thus, it seems likely that RI, RIII, and RIV are not expressed in LSEC.

Quantitative precipitin curve and SIC characterization

We prepared SIC using a quantitative precipitin curve described 76 y ago by Heidelberger and Kendall (5). Calibrating a single lot of affinity-purified rabbit IgG anti-OVA Ab, we determined the concentrations of Ab and OVA at the POE where the immune complexes precipitated maximally (Fig. 7A). We then prepared SIC at a concentration of Ag 15-fold greater than the POE concentration, conditions found by others to yield SIC (2, 3, 5). Measured by DLS, these SIC had a mean diameter by volume of \sim 39 nm with a range from 20 to 150 nm (Fig. 7B).

SIC are not cleared efficiently in the RIIB KO mouse strain

Testing a prediction of our central hypothesis, that the RIIB of LSEC serves the purpose of removing SIC from circulation, we measured the elimination rate of SIC from the bloodstream of both WT and RIIB KO strains. Mice were infused by tail vein with trace radio-iodinated SIC prepared at 15 times Ag excess, as described earlier; the decay of gamma-radiation from peripheral

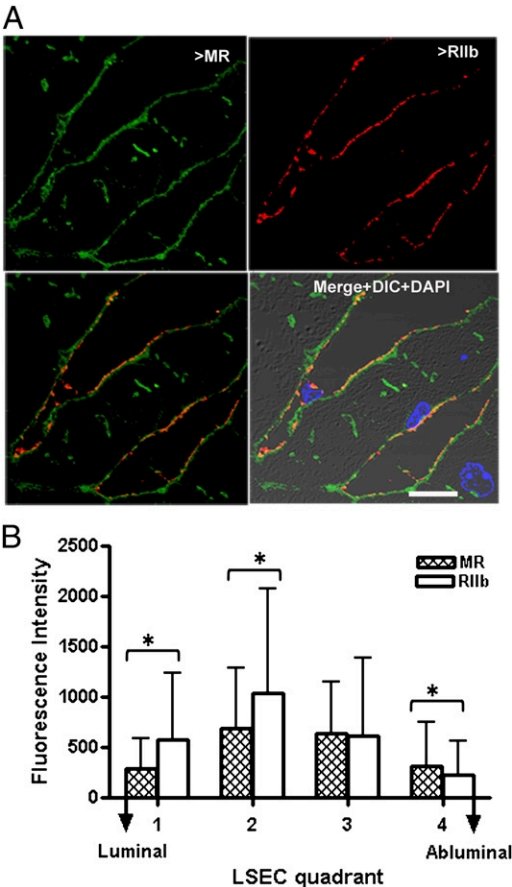


FIGURE 4. LSEC RIIB is mostly in the membrane. (A) Two-color IF images of an ultrathin (100 μ m) cryosection through mouse liver locating the binding of anti-MR (green, *upper left*) and anti-RIIB (red, *upper right*). The *bottom panels* show merged images of the *upper two panels*, and the *right lower panel* adds DIC and DAPI staining. Scale bar, 10 μ m. (B) Quantification of relative topological distribution of RIIB and MR in LSEC. The bar graph plots the fluorescence intensities (mean \pm SD) of the two colors in LSEC cross-sections drawn from luminal to abluminal surfaces. n = 100 sinusoids. $*p$ < 0.05.

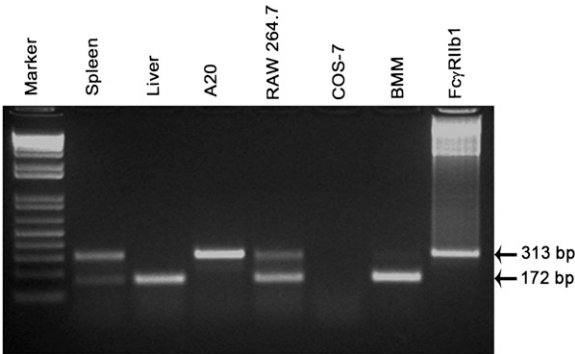


FIGURE 5. The RIIB isoform expressed in liver is b2. Ethidium bromide-stained agarose gel of electrophoresed RT-PCR products using primers specific for RIIB showing the mRNA expression of the two RIIB isoforms in organs and cells including spleen, liver, A20, RAW 264.7, COS-7, M-CSF-differentiated BMM, and b1 cDNA. The two bands at 313 and 172 bp correspond to the two RIIB transcripts b1 and b2, respectively. The data are representative of samples from two sets of WT organs and cell line preparations.

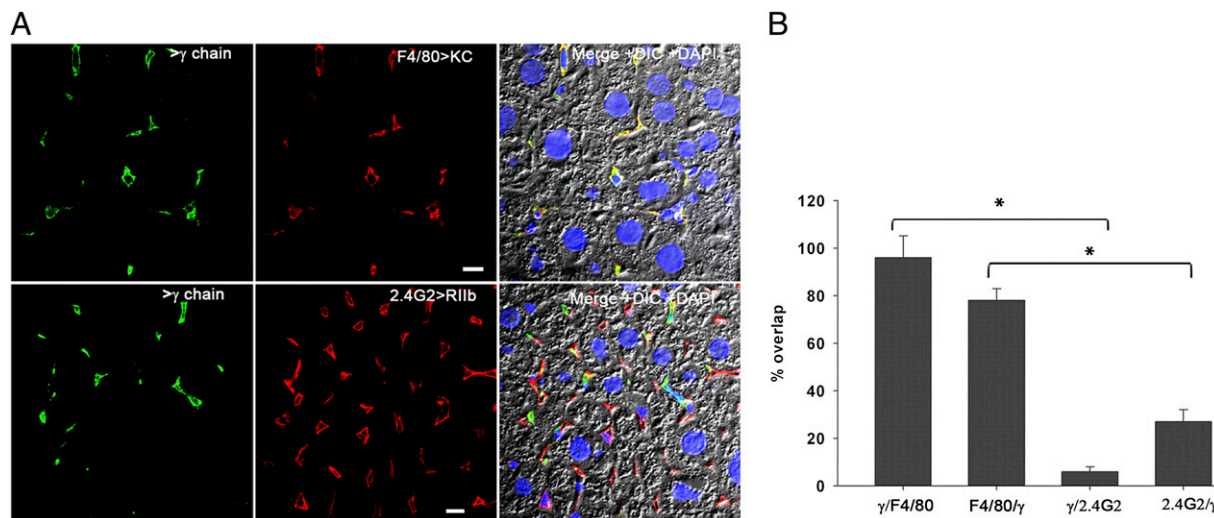


FIGURE 6. Fc γ -chain is expressed only in KC and not in LSEC. **(A)** The confocal IF image in the *left column* illustrates the expression pattern of γ -chain (green). The *middle column* shows the location of KC shown using anti-F4/80 (red) in the *top panel* and the location of LSEC using mab anti-2.4G2 (red) in the *bottom panel*. The merged color image shows the colocalization of signal from γ -chain with signals from F-4/80 and 2.4G2 along with DIC and DAPI staining of nuclei. Scale bars, 10 μ m. **(B)** Quantitative colocalization analysis was applied to all images represented in (A). The graph represents the percentage of signal from γ -chain Ab (green) colocalizing with signal from F4/80 or 2.4G2 (red) Ab and vice versa in the *top panel* of (A) and also for the *bottom panel* (mean \pm SD). Using a random-effects linear regression model, the data from bars 1 and 3 and also between bar 2 and 4 were analyzed. * $p < 0.001$.

blood was followed over the course of 1 h; and the data in cpm were plotted in semilogarithmic fashion (Fig. 8). Indeed, our prediction was not falsified. Rather, we found that the rate of SIC clearance from the RIIb KO strain was dramatically retarded compared with the WT strain. Specifically, both curves described biexponential decay with early and late phases. Decay was most obvious during the late phase, from 10 to 60 min, where half-lives were 87 ± 20 min and 367 ± 222 min for WT and KO mice, respectively (mean \pm SD, $n = 5$ to 6, $p = 0.0001$), indicating a 3-fold lengthier survival of SIC in the absence of RIIb. In contrast, decay rates during the early 1- to 5-min period were not statistically different between the two strains, half-lives for WT and RIIb KO strains being 12 ± 6 min and 19 ± 10 min, respectively ($n = 5$ to 6, $p = 0.2$) (Fig. 8). Note also that the cpm at 1 min were $>20\%$ lower in WT compared with the KO strain (see *Discussion*).

Quantification of SIC in various organs

Documenting that infused SIC homes mostly to liver, we autopsied three mice 25 min after infusion of radio-iodinated SIC. Of the total administered dose, we recovered $72 \pm 2\%$ in blood, $27 \pm 2\%$ in liver, $0 \pm 1\%$ in lung, $1 \pm 0\%$ in spleen, and $0 \pm 1\%$ in kidney (mean \pm SD). Thus, nearly all of the cleared SIC (96%) was found in the liver.

Discussion

Our results allow two major conclusions. First, RIIb is highly expressed on the endothelial cells of the liver sinusoids. This impression is easily reached by simple inspection of a section of liver stained with anti-RIIb Ab. But, wanting to quantify our visual impression, we have measured by immunoblotting the amount of RIIb expressed in the major organs of the body and have concluded that

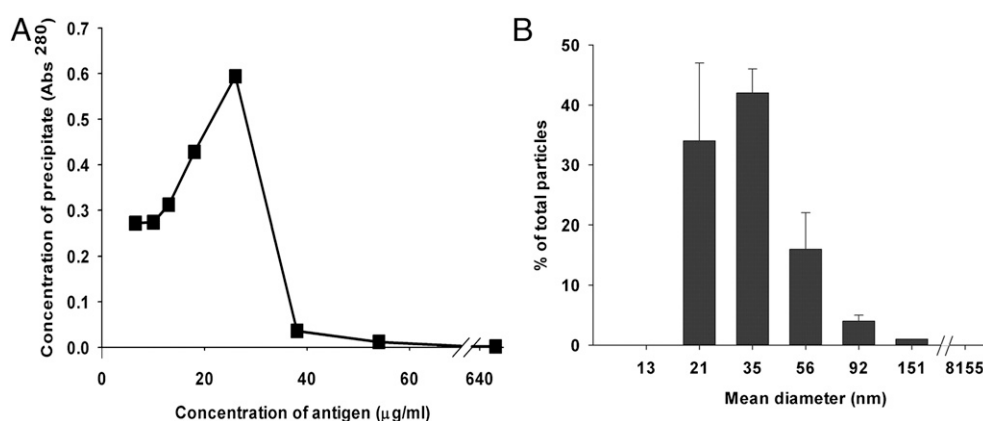


FIGURE 7. **(A)** Quantitative precipitin curve. The graph shows a quantitative precipitin curve plotting the protein concentrations of immune precipitates (pellets) from a series of tubes incubating increasing concentrations of Ag and a fixed concentration of Ab. The peak marks the POE. **(B)** Particle size measurement. Particle size distribution of SIC prepared at a 15-fold Ag excess was measured using DLS; the data obtained with Dynapro software are presented. The graph plots particle mean (\pm variance) diameter in nm on the x-axis, and the y-axis shows the percent distribution of total particles calculated using the relative amount of particles [$G(d)$] at each size.

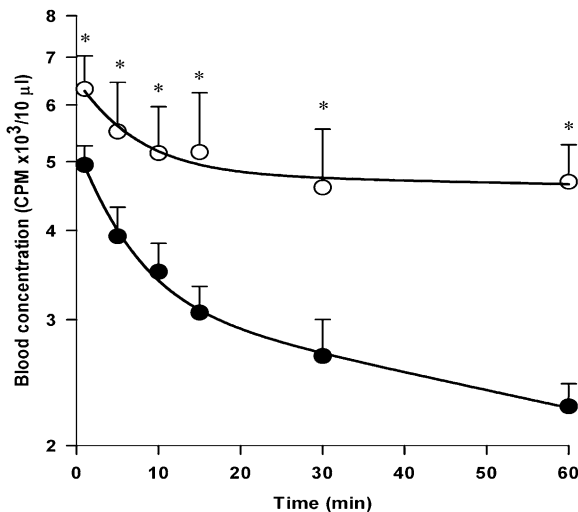


FIGURE 8. SIC are not cleared efficiently in the RIIb KO mouse strain. We infused via the tail vein radio-iodinated SIC prepared at $15\times$ Ag excess of POE and then evaluated the clearance of SIC from peripheral blood by counting gamma-radiation in blood collected from the retro-orbital sinuses. The curve plots mean \pm SD values of SIC in blood samples, after adjustment for dose/body weight (see *Materials and Methods*), over time from six WT (closed circle) and five RIIb KO (open circle) animals combining all data from two experiments done 3 mo apart. * $p < 0.05$ (statistically significant differences between strain values at each time point; Student t test).

the fraction of total RIIb on LSEC is astonishingly high, about three-quarters of the total RIIb in the body. Relatively small fractions of the total are noted in spleen and blood and bone marrow. It should be acknowledged that we have not sampled all organs, so our total value may be somewhat underestimated, but in fact we have sampled all of the major immune system organs and would conclude that the liver content is far in excess of that of any other organ.

The second major conclusion to be derived from our data is that RIIb of the liver sinusoidal endothelium is responsible for removing SIC from blood. This follows from our observation that the elimination rate of SIC from blood of the RIIb KO strain was severely diminished. Three elements of this conclusion require comment. First, we contend that the liver is the major organ removing SIC. This contention is supported by our observations 1) that the RIIb KO mouse is severely deficient in eliminating SIC, 2) that the majority of RIIb of the mouse is expressed in the liver, and 3) that in our hands 96% of cleared SIC is found in the liver by direct gamma-counting. Further, the literature supports this conclusion with abundant direct data showing liver clearance of the major fraction of blood-borne SIC (1, 3, 4, 15, 39, 40). The spleen, contrary to conventional wisdom, is only a minor participant in SIC elimination.

The second element of our second major conclusion is that RIIb is the operant Fc γ R responsible for liver clearance. This observation is remarkable because this receptor has been known almost exclusively as an inhibiting receptor, downmodulating the immune complex-mediated effects of the other agonist receptors in its gene family. By contrast, here in our studies it functions as an agonist. Early work, however, indicated that it was indeed capable of agonist activity, specifically of pinocytotic uptake of ligand; but these were *in vitro* experiments and not *in vivo* as ours are (41–43). We know of one other situation where this receptor appears to act alone, without an associated receptor, and that is to produce apoptosis when clustered on B cells (44). The mechanistic details of how RIIb acts on LSEC to eliminate immune complexes will require further study.

The third remarkable element of our second major conclusion is that a specialized endothelium, the LSEC, is the predominant cell responsible for SIC elimination in that 90% of liver RIIb is expressed on LSEC. The LSEC, according to the literature, is a vigorous scavenger of bloodstream detritus, expressing a variety of surface receptors for blood-borne material, displaying abundant coated vesicles and lysosomes appropriate for a disposal mechanism (45), and in our hands eliminating blood-borne virus with remarkable efficiency (12). Further, the uptake of immune complex by LSEC has been well documented by others (4, 13, 16, 46). We note parenthetically that Fc γ R-expressing endothelium has been found elsewhere only in the human placenta, and there, too, the isoform expressed is RIIb (28).

The absence of the small fraction (10%) of total liver RIIb expressed on KC cannot be responsible for the slow rate of immune complex elimination in the RIIb KO mouse. Rather, the absence of RIIb on KC would be predicted to render the KC more vigorously endocytic due to overactive agonistic Fc γ R unopposed by the inhibitory RIIb. The result would be a more rapid decay of blood-borne SIC in the KO strain compared with the WT strain, the exact reverse of what we found.

We find the decay kinetics of SIC in the RIIb KO strain noteworthy on two accounts. First is the striking decrease in the rate of elimination during the latter of the two biexponential elimination phases, from 5 to 60 min, indicating that RIIb is largely responsible for the removal of blood-borne SIC. Second is the observation that the 1-min point on the WT curve is $>20\%$ lower than the 1-min point of the KO curve ($p = 0.002$, Fig. 8) despite the strains not only being matched for age and sex but also adjusted for radioisotope dose and body weight; and, further, that the period from 1 to 5 min shows similar rates of decay in both strains. We interpret these kinetics to suggest that during the first minute after infusion, the LSEC RIIb become saturated with SIC that pinocytose into (likely) coated vesicles, disappearing from the LSEC surface such that for the next 5 min, no more RIIb-specific elimination occurs. Then, after 5 min, RIIb begin to reappear on the LSEC surface, either by re-expression of endocytosed receptor, suggested by others (16), or by biosynthesis; and an ongoing elimination of SIC ensues at a vigorous rate (half-life ~ 90 min). This supposition suggests a fruitful path of insight into the mechanism of elimination and warrants detailed investigation.

We call attention to old observations that the repetitive infusion of SIC, such as those used here in our study, causes serum sickness with characteristic microscopic findings of glomerulonephritis (6, 7, 47). We speculate that LSEC RIIb, mediating the elimination of SIC, may critically attenuate the manifestations of serum sickness. One would further anticipate that a strain of mouse lacking only LSEC RIIb may be more susceptible to serum sickness and other soluble immune complex-mediated diseases, whereas targeted elimination of RIIb in B cells and myeloid cells would not produce like effects. Likewise, animals harboring mutants of the RIIb gene that result in diminished or defective receptor expression may as well be more susceptible to immune complex-mediated diseases. Such mutants have been described although their analyses appear to have focused on B cell and myeloid RIIb expression, whereas the evaluation of RIIb expression on LSEC would be expected to reveal more telling results (20, 48, 49).

Summarizing for clarity, risking oversimplification, we would propose that SIC are constitutively eliminated by LSEC RIIb, but when this capacity is overwhelmed, the escaping immune complexes become large and lodge in end organs to result in disease. Alterations in the expression and function of RIIb would modify this course of events.

Acknowledgments

We thank Dr. Sara Cole, Richard Montione, Brian Kemmenoe, and the staff at The Ohio State University Campus Microscopy and Imaging Facility for training and advice and Dr. John Cambier, University of Colorado, and Dr. Mark Coggeshall, Oklahoma Medical Research Foundation, for Abs against mouse RIIb.

Disclosures

The authors have no financial conflicts of interest.

References

- Benacerraf, B., M. Sebestyen, and N. S. Cooper. 1959. The clearance of antigen antibody complexes from the blood by the reticuloendothelial system. *J. Immunol.* 82: 131–137.
- Arend, W. P., and J. C. Sturge. 1979. Composition and biologic properties of soluble IgG-anti-IgG immune complexes: effects of variations in the specificity of rabbit antibodies to different structural components of human IgG. *J. Immunol.* 123: 447–454.
- Kurlander, R. J., D. M. Ellison, and J. Hall. 1984. The blockade of Fc receptor-mediated clearance of immune complexes in vivo by a monoclonal antibody (2.4G2) directed against Fc receptors on murine leukocytes. *J. Immunol.* 133: 855–862.
- Skogh, T., R. Blomhoff, W. Eskild, and T. Berg. 1985. Hepatic uptake of circulating IgG immune complexes. *Immunology* 55: 585–594.
- Heidelberger, M., and F. E. Kendall. 1935. A quantitative theory of the precipitin reaction: III. The reaction between crystalline egg albumin and its homologous antibody. *J. Exp. Med.* 62: 697–720.
- Dixon, F. J., J. J. Vazquez, W. O. Weigle, and C. G. Cochrane. 1958. Pathogenesis of serum sickness. *AMA Arch. Pathol.* 65: 18–28.
- McCluskey, R. T., B. Benacerraf, J. L. Potter, and F. Miller. 1960. The pathologic effects of intravenously administered soluble antigen-antibody complexes. I. Passive serum sickness in mice. *J. Exp. Med.* 111: 181–194.
- Haakenstad, A. O., G. E. Striker, and M. Mannik. 1982. The disappearance kinetics and glomerular deposition of small-latticed soluble immune complexes. *Immunology* 47: 407–414.
- Wener, M. H., and M. Mannik. 1986. Mechanisms of immune deposit formation in renal glomeruli. *Springer Semin. Immunopathol.* 9: 219–235.
- Hebert, L. A., D. J. Birmingham, F. G. Cosio, and D. D. Sedmak. 1994. Circulating immune complexes. In *Immunochimistry*. C. J. van Oss, and M. H. V. van Regenmortel, eds. Marcel Dekker, New York, p. 653–680.
- Ravetch, J. V., and R. A. Clynes. 1998. Divergent roles for Fc receptors and complement in vivo. *Annu. Rev. Immunol.* 16: 421–432.
- Ganesan, L. P., S. Mohanty, J. Kim, K. R. Clark, J. M. Robinson, and C. L. Anderson. 2011. Rapid and efficient clearance of blood-borne virus by liver sinusoidal endothelium. *PLoS Pathog.* 7: e1002281.
- Muro, H., H. Shirasawa, Y. Takahashi, M. Maeda, and S. Nakamura. 1988. Localization of Fc receptors on liver sinusoidal endothelium. A histological study by electron microscopy. *Acta Pathol. Jpn.* 38: 291–301.
- Pulford, K., E. Ralfkiaer, S. M. MacDonald, W. N. Erber, B. Falini, K. C. Gatter, and D. Y. Mason. 1986. A new monoclonal antibody (KB61) recognizing a novel antigen which is selectively expressed on a subpopulation of human B lymphocytes. *Immunology* 57: 71–76.
- Kosugi, I., H. Muro, H. Shirasawa, and I. Ito. 1992. Endocytosis of soluble IgG immune complex and its transport to lysosomes in hepatic sinusoidal endothelial cells. *J. Hepatol.* 16: 106–114.
- Mousavi, S. A., M. Sporstøl, C. Fladeby, R. Kjekshus, N. Barois, and T. Berg. 2007. Receptor-mediated endocytosis of immune complexes in rat liver sinusoidal endothelial cells is mediated by FcγRIIb2. *Hepatology* 46: 871–884.
- March, S., E. E. Hui, G. H. Underhill, S. Khetani, and S. N. Bhatia. 2009. Microenvironmental regulation of the sinusoidal endothelial cell phenotype in vitro. *Hepatology* 50: 920–928.
- Ahmed, S. S., H. Muro, M. Nishimura, I. Kosugi, Y. Tsutsi, and H. Shirasawa. 1995. Fc receptors in liver sinusoidal endothelial cells in NZB/W F1 lupus mice: a histological analysis using soluble immunoglobulin G-immune complexes and a monoclonal antibody (2.4G2). *Hepatology* 22: 316–324.
- Nimmerjahn, F., and J. V. Ravetch. 2007. Fc-receptors as regulators of immunity. *Adv. Immunol.* 96: 179–204.
- Smith, K. G. C., and M. R. Clatworthy. 2010. FcγRIIb in autoimmunity and infection: evolutionary and therapeutic implications. *Nat. Rev. Immunol.* 10: 328–343.
- Takai, T., M. Ono, M. Hikida, H. Ohmori, and J. V. Ravetch. 1996. Augmented humoral and anaphylactic responses in FcγRII-deficient mice. *Nature* 379: 346–349.
- Ganesan, L. P., G. Wei, R. A. Pengal, L. Moldovan, N. Moldovan, M. C. Ostrowski, and S. Tridandapani. 2004. The serine/threonine kinase Akt promotes Fcγ receptor-mediated phagocytosis in murine macrophages through the activation of p70S6 kinase. *J. Biol. Chem.* 279: 54416–54425.
- Raab, M., S. Kappel, A. Krämer, Y. Matthess, E. Kurunci-Csacsko, J. Calzada-Wack, B. Rathkolb, J. Rozman, T. Adler, et al. 2011. Toxicity modelling of Plk1-targeted therapies in genetically engineered mice and cultured primary mammalian cells. *Nat Commun* 2: 395.
- Cao, G., R. S. Clark, W. Pei, W. Yin, F. Zhang, F. Y. Sun, S. H. Graham, and J. Chen. 2003. Translocation of apoptosis-inducing factor in vulnerable neurons after transient cerebral ischemia and in neuronal cultures after oxygen-glucose deprivation. *J. Cereb. Blood Flow Metab.* 23: 1137–1150.
- Rondinelli, R. H., D. E. Epner, and J. V. Tricoli. 1997. Increased glyceraldehyde-3-phosphate dehydrogenase gene expression in late pathological stage human prostate cancer. *Prostate Cancer Prostatic Dis.* 1: 66–72.
- Pikula, S., J. Bandorowicz-Pikula, S. Awasthi, and Y. C. Awasthi. 1996. Differential staining of human erythrocyte membrane proteins by Coomassie and silver: implications in the assessment of homogeneity of membrane proteins. *Biochem. Arch.* 12: 237–243.
- Takizawa, T., K. Suzuki, and J. M. Robinson. 1998. Correlative microscopy using FluoroNanogold on ultrathin cryosections. Proof of principle. *J. Histochem. Cytochem.* 46: 1097–1102.
- Takizawa, T., C. L. Anderson, and J. M. Robinson. 2005. A novel FcγRII receptor-defined, IgG-containing, compartment in placental endothelium. *J. Immunol.* 175: 2331–2339.
- Mori, M., G. Ishikawa, T. Takeshita, T. Goto, J. M. Robinson, and T. Takizawa. 2006. Ultra-high-resolution immunofluorescence using ultrathin cryosections: subcellular distribution of caveolin-1 and CD31 in human placental endothelial cells. *J. Electron Microsc. (Tokyo)* 55: 107–112.
- Takizawa, T., and J. M. Robinson. 2006. Correlative microscopy of ultrathin cryosections in placental research. *Methods Mol. Med.* 121: 351–369.
- Manders, E. M. M., F. J. Verbeek, and J. A. Aten. 1993. Measurement of co-localization of objects in dual-colour confocal images. *J. Microsc.* 169: 375–382.
- Mohanty, S., J. Kim, L. P. Ganesan, G. S. Phillips, K. Hua, D. Jarjoura, W. L. Hayton, J. M. Robinson, and C. L. Anderson. 2010. IgG is transported across the mouse yolk sac independently of FcγRIIb. *J. Reprod. Immunol.* 84: 133–144.
- Maurer, P. H. 1971. Precipitation reactions. In *Methods in Immunology and Immunochimistry*. C. A. Williams, and M. W. Chase, eds. Academic Press, New York, London, p. 1–58.
- Duta, F., M. Ulanova, D. Seidel, L. Puttagunta, S. Musat-Marcu, K. S. Harrod, A. D. Schreiber, U. Steinhoff, and A. D. Befus. 2006. Differential expression of spleen tyrosine kinase Syk isoforms in tissues: Effects of the microbial flora. *Histochem. Cell Biol.* 126: 495–505.
- Muro, H., H. Shirasawa, M. Maeda, and S. Nakamura. 1987. Fc receptors of liver sinusoidal endothelium in normal rats and humans. A histologic study with soluble immune complexes. *Gastroenterology* 93: 1078–1085.
- Wirthmueller, U., T. Kurosaki, M. S. Murakami, and J. V. Ravetch. 1992. Signal transduction by FcγRIII (CD16) is mediated through the gamma chain. *J. Exp. Med.* 175: 1381–1390.
- Miller, K. L., A.-M. Duchemin, and C. L. Anderson. 1996. A novel role for the Fc receptor gamma subunit: enhancement of FcγRII ligand affinity. *J. Exp. Med.* 183: 2227–2233.
- Nimmerjahn, F., P. Bruhns, K. Horiuchi, and J. V. Ravetch. 2005. FcγRIV: A novel FcR with distinct IgG subclass specificity. *Immunity* 23: 41–51.
- Haakenstad, A. O., and M. Mannik. 1976. The disappearance kinetics of soluble immune complexes prepared with reduced and alkylated antibodies and with intact antibodies in mice. *Lab. Invest.* 35: 283–292.
- Finbloom, D. S., and P. H. Plotz. 1979. Studies of reticuloendothelial function in the mouse with model immune complexes. I. Serum clearance and tissue uptake in normal C3H mice. *J. Immunol.* 123: 1594–1599.
- Miettinen, H. M., J. K. Rose, and I. Mellman. 1989. Fc receptor isoforms exhibit distinct abilities for coated pit localization as a result of cytoplasmic domain heterogeneity. *Cell* 58: 317–327.
- Miettinen, H. M., K. Matter, W. Hunziker, J. K. Rose, and I. Mellman. 1992. Fc receptor endocytosis is controlled by a cytoplasmic domain determinant that actively prevents coated pit localization. *J. Cell Biol.* 116: 875–888.
- Van Den Herik-Oudijk, I. E., N. A. C. Westerdal, N. V. Henriquez, P. J. A. Capel, and J. G. J. Van De Winkel. 1994. Functional analysis of human FcγRII (CD32) isoforms expressed in B lymphocytes. *J. Immunol.* 152: 574–585.
- Pearse, R. N., T. Kawabe, S. Bolland, R. Guinamard, T. Kurosaki, and J. V. Ravetch. 1999. SHIP recruitment attenuates FcγRIIb-induced B cell apoptosis. *Immunity* 10: 753–760.
- Elvevold, K., B. Smedsrød, and I. Martinez. 2008. The liver sinusoidal endothelial cell: a cell type of controversial and confusing identity. *Am. J. Physiol. Gastrointest. Liver Physiol.* 294: G391–400.
- van der Laan-Klamer, S. M., J. E. Atmosoerodjo-Briggs, G. Harms, P. J. Hoedemaeker, and M. J. Hardonk. 1985. A histochemical study about the involvement of rat liver cells in the uptake of heterologous immune complexes from the circulation. *Histochemistry* 82: 477–482.
- Benacerraf, B., J. L. Potter, R. T. McCluskey, and F. Miller. 1960. The pathologic effects of intravenously administered soluble antigen-antibody complexes. II. Acute glomerulonephritis in rats. *J. Exp. Med.* 111: 195–200.
- Stefanescu, R. N., M. Olferiev, Y. Liu, and L. Pricop. 2004. Inhibitory Fcγ receptors: from gene to disease. *J. Clin. Immunol.* 24: 315–326.
- Su, K., H. Yang, X. Li, X. Li, A. W. Gibson, J. M. Cafardi, T. Zhou, J. C. Edberg, and R. P. Kimberly. 2007. Expression profile of FcγRIIb on leukocytes and its dysregulation in systemic lupus erythematosus. *J. Immunol.* 178: 3272–3280.